A Switching Control Perspective on the Offshore Construction Scenario of Heavy-Lift Vessels

Ye, Jun; Roy, Spandan; Godjevac, Milinko; Baldi, Simone

DOI
10.1109/TCST.2020.2978446

Publication date
2021

Document Version
Accepted author manuscript

Published in
IEEE Transactions on Control Systems Technology

A Switching Control Perspective on the Offshore Construction Scenario of Heavy-Lift Vessels

Jun Ye, Spandan Roy, Milinko Godjevac and Simone Baldi

***Abstract*—Position control for heavy-lift construction vessels is crucial for safe operation during offshore construction. During the various phases of a typical offshore construction assignment considerable changes in the dynamics of the crane-vessel system occur. Operational hazard was reported if such interchanging dynamics are not properly handled. However, to date and to the best of the authors' knowledge, no systematic control solution is reported considering multi-phase offshore construction scenarios. This paper proposes a switched dynamical framework to model the interchanging phases and to formulate a comprehensive position control solution for heavy-lift vessels. Stability and robustness against modelling imperfections and environmental disturbances are analytically assessed. The effectiveness of the solution is verified on a realistic heavy-lift vessel simulation platform: it is shown that the proposed switched framework sensibly improves accuracy and reduces hazard as compared to a non-switched solution designed for only one phase of the construction scenario.**

***Index Terms*—Dynamic positioning system, Heavy-lift construction vessel, Switched systems, Observer-based control.**

I. Introduction

With the development of the offshore energy industry, construction works such as installation and removal of offshore structures in deep ocean have been increasing [1]. During such construction works, a heavy-lift construction vessel must operate close to some offshore platform: the position of the vessel should be controlled via Dynamic Positioning (DP) acting on the propulsion system [2], [3], in such a way to avoid any operational hazard, i.e. to avoid the vessel to come too close to the platform or hit it. A few reports have appeared showing that DP systems for heavy-lift vessels can go unstable in certain phases of the offshore construction due to the time-varying vessel-load dynamics and the large uncertainties in the system [4]–[7]. Although details are often confidential and DP design are rarely disclosed, it is known that special DP functions (heavy lift mode, external force compensation mode) are devised by DP providers to handle such critical scenarios [8], [9]. A motivating example is illustrated below.

This work is financially supported by the China Scholarship Council (CSC) project No. 20167720003, by the Fundamental Research Funds for the Central Universities grant no. 4007019109, and by the special guiding funds double first-class grant no. 4007019201 (corresponding author: S. Baldi)

J. Ye is with Dep. of Maritime and Transport Technology, Delft Univ. of Technology (TU Delft), Delft 2628 CD, Netherlands e-mail: j.ye-1@tudelft.nl

S. Roy is with Robotics Research Centre, International Institute of Information Technology Hyderabad, India, and with Delft Center for Systems & Control, TU Delft, Delft 2628 CD, Netherlands e-mail: spandan.roy@iiit.ac.in

M. Godjevac is with Allseas Group S.A., Poortweg 12, 2612PA, The Netherlands e-mail: MGj@allseas.com.

S. Baldi is with School of Mathematics, Southeast University, Nanjing 210096, China, and guest with Delft Center for Systems & Control, TU Delft, Delft 2628 CD, Netherlands e-mail: s.baldi@tudelft.nl

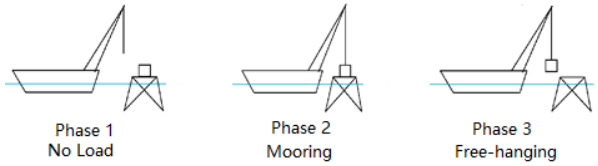

Figure 1: Schematics of various phases during a typical offshore removal assignment (in installation assignment Phases 3 and 1 occur in opposite order).

A. Motivational Example: Construction Assignment

Typical offshore construction assignments include offshore installation and removal [5], [6]. If we consider the offshore removal as an example, it consists of three phases, sketched in Fig. 1: (i) in the first phase, the vessel sails to the desired position without load (free-floating); (ii) in the second phase, the vessel lifts a load from a platform, where it encounters the so-called 'mooring force' (external stiffness on the crane wires); (iii) the third phase is the 'free-hanging' condition, where the load is hanging from the crane. Clearly, the overall mass of the vessel changes during the interchange of these phases. Moreover, the mooring force is only active during Phase 2. Currently, no DP solution can tackle the interchanging dynamics during a complete offshore construction assignment [4]–[7]. Let us discuss research attempts in this direction, together with the contribution brought by this research.

B. Related Works and Contribution

The research on control solutions for DP systems can be broadly classified into three categories: *(i)* approaches that consider environmental disturbances (wind/waves) as the only source of uncertainty, but ignore modelling uncertainty [2], [10], [11]; *(ii)* approaches that tackle modelling uncertainty via robust [12]–[17] or adaptive [18]–[22] control theory, but ignore that high-frequency environmental disturbances and measurement noises hit the limits of marine thrusters (such thrusters are slow due to the large size of the ship and cannot deliver high-frequency commands) and *(iii)* approaches that filter high-frequency disturbance via observers but ignore modelling uncertainty [23], [24].

Based on the above discussion, a novel switching control perspective is proposed in this work which overcomes the stability, robustness and filtering limitations of the state of the art. The main contributions are:

- A *switched dynamics* is formulated which suitably capture the interchanging dynamics during various operational phases of an offshore vessel in a compact manner.

- Based on the switched dynamics, an observer-based *switched control solution* is proposed which can effectively tackle the interchanging dynamics even in the presence of model imperfections and high-frequency disturbances. Stability and robustness are analytically assessed.
- The effectiveness of the framework is verified via a heavy-lift vessel simulation platform which, to the best of our knowledge, is the first one capable of *simulating the interchanging dynamics in six degrees of freedom*.

The paper is organized as follows: in Section II, the switched dynamics and DP control problem are formulated; Section III presents the proposed control scheme along with its stability analysis; Section IV presents the simulations and Section V concludes the work.

Following notations are used: $\lambda_{\min}(\bullet)$ and $||\bullet||$ represent the minimum eigenvalue and Euclidean norm of $(\bullet)$ respectively; $\mathbf{I}$ denotes identity matrix with appropriate dimension; $\mathbf{\Xi} > \mathbf{0}$ denotes a positive definite matrix $\mathbf{\Xi}$; $diag\{\cdot, \cdots, \cdot\}$ denote a diagonal matrix with diagonal elements $\{\cdot, \cdots, \cdot\}$. Let us also denote the integration variable with the symbol ϖ.

II. System Dynamics and Problem Formulation

Usually, a DP system can only control the movement of vessels in surge, sway and yaw. Therefore, DP literature commonly adopts the following three degrees-of-freedom (DoFs) crane-vessel model [25], [26]:

$$\dot{\boldsymbol{\eta}}(t) = \mathbf{J}(\psi(t))\boldsymbol{\nu}(t), \tag{1}$$

$$\mathbf{M}\dot{\boldsymbol{\nu}}(t) = -\mathbf{D}\boldsymbol{\nu}(t) + \boldsymbol{\tau}_c(t) + \boldsymbol{\tau}(t) + \boldsymbol{\tau}_l(t) + \bar{\mathbf{d}}(t), \tag{2}$$

where $\mathbf{J}(\psi(t)) = \begin{bmatrix} \cos(\psi(t)) & -\sin(\psi(t)) & 0 \\ \sin(\psi(t)) & \cos(\psi(t)) & 0 \\ 0 & 0 & 1 \end{bmatrix}$, the state $\boldsymbol{\eta} = [x, y, \psi]^T$ comprises of north position, east position and heading angle of the ship in earth-fixed coordinate system, respectively; $\boldsymbol{\nu} = [u, v, r]^T$ is the vessel velocity/angular velocity in body-fixed coordinate system; $\mathbf{M} \in \mathbb{R}^{3\times3}$ is the mass/inertia matrix; $\mathbf{D} \in \mathbb{R}^{3\times3}$ denotes the damping matrix; $\bar{\mathbf{d}} \in \mathbb{R}^3$ denotes bounded environmental disturbances representing the effects of wind, wave and current forces; $\boldsymbol{\tau} \in \mathbb{R}^3$ is the generalized control input to be designed; $\boldsymbol{\tau}_c \in \mathbb{R}^3$ denotes the force from the crane winch controlling the crane wires; $\boldsymbol{\tau}_l \in \mathbb{R}^3$ denotes bounded force from the hanging of the load.

Table I: The Three Phases in Offshore Heavy-Lift Operation

Phase 1: No Load	$\boldsymbol{\tau}_c(t) = \mathbf{0},\ \boldsymbol{\tau}_l(t) = \mathbf{0}.$
Phase 2: Mooring	$\boldsymbol{\tau}_c(t) = -\mathbf{F}\boldsymbol{\eta}(t),\ \boldsymbol{\tau}_l(t) = \mathbf{0}.$
Phase 3: Free-hanging	$\boldsymbol{\tau}_c(t) = \mathbf{0},\ \boldsymbol{\tau}_l(t) \neq \mathbf{0}$

Based on the construction work scenario depicted in Fig. 1, the crane-vessel system (1)-(2) undergoes at least three main structural changes summarized in Table I and denoted with the terms Phase 1 "No load", Phase 2 "Mooring mode" and Phase 3 "Free-hanging mode". During Phase 2 the crane wires are attached to the load, resulting in a spring-type force (mooring force). During Phase 3 the load acts as an external disturbance. The load will also affect the mass matrix in Phases 2 and 3.

A. Switching-based Modelling

The structural changes of (1)-(2) summarized in Table I can be compactly captured by a switched dynamical framework

$$\dot{\boldsymbol{\eta}}(t) = \mathbf{J}(\psi(t))\boldsymbol{\nu}(t), \tag{3}$$

$$\begin{aligned} \mathbf{M}_{\sigma(t)}\dot{\boldsymbol{\nu}}(t) &= -\mathbf{D}\boldsymbol{\nu}(t) - \mathbf{F}_{\sigma(t)}\boldsymbol{\eta}(t) \\ &\quad + \boldsymbol{\tau}_{\sigma(t)}(t) + \bar{\mathbf{d}}(t) + \boldsymbol{\tau}_{l\sigma(t)}(t) \\ \Rightarrow \dot{\boldsymbol{\nu}}(t) &= -\mathbf{A}_{1\sigma(t)}\boldsymbol{\eta}(t) - \mathbf{A}_{2\sigma(t)}\boldsymbol{\nu}(t) \\ &\quad + \mathbf{M}^{-1}_{\sigma(t)}\boldsymbol{\tau}_{\sigma(t)}(t) + \mathbf{d}_{\sigma(t)}(t), \end{aligned} \tag{4}$$

where $\sigma(\cdot)$ is a piece-wise constant *switching signal* taking values in $\{1, 2, 3\} = \Omega$, i.e. selecting which phase is active. In particular, $\mathbf{F}_1 = \mathbf{F}_3 = \mathbf{0}$, $\boldsymbol{\tau}_{11} = \boldsymbol{\tau}_{l2} = \mathbf{0}$ (cf. Table I), and

$$\mathbf{A}_{1\sigma(t)} \triangleq \mathbf{M}^{-1}_{\sigma(t)}\mathbf{F}_{\sigma(t)}, \tag{5}$$

$$\mathbf{A}_{2\sigma(t)} \triangleq \mathbf{M}^{-1}_{\sigma(t)}\mathbf{D}, \tag{6}$$

$$\mathbf{d}_{\sigma(t)}(t) \triangleq \mathbf{M}^{-1}_{\sigma(t)}(\bar{\mathbf{d}}(t) + \boldsymbol{\tau}_{l\sigma(t)}(t)). \tag{7}$$

To describe the duration of the different phases following one another, the following class of switching signals is considered:

Definition 1. *(Average Dwell Time (ADT) [27]): For a switching signal $\sigma(\cdot)$ and each $t_2 \geq t_1 \geq 0$, let $N_\sigma(t_1, t_2)$ denote the number of discontinuities in the interval $[t_1, t_2)$. Then $\sigma(\cdot)$ has an average dwell time ϑ if for a given scalar $N_0 > 0$*

$$N_\sigma(t_1, t_2) \leq N_0 + (t_2 - t_1)/\vartheta, \quad \forall t_2 \geq t_1 \geq 0, \tag{8}$$

where N_0 is termed as chatter bound, indicating the number of switching instants over intervals shorter than ϑ.

Remark 1 (The rationale for ADT)**.** *The ADT concept is well known in switching control literature [27]–[30]. In offshore DP setting, this concept can be used to define the average duration of the different phases, which might depend on application requirements. Consider, for example: Phase 1 = 10 min, Phase 2 = 20 min, Phase 3 = 5 min [1], [6]. This can be described by* (8) *with $\vartheta \approx 12$ min and $N_0 \approx 2$, indicating that on average there is one phase change every 12 min and at most 2 phase changes over intervals shorter than 12 min.*

B. Uncertainty description

The external disturbance is upper bounded as $||\mathbf{d}_\sigma(t)|| \leq ||\Delta\mathbf{d}_\sigma||\ \forall t$ where $||\Delta\mathbf{d}_\sigma||$ is available for control design. For each phase, the mass matrix $\mathbf{M}_\sigma$ is assumed to be known for control design, under the standard assumption that added mass terms are negligible during DP operation[1]. However, $\mathbf{F}_\sigma$ and $\mathbf{D}$ cannot be assumed to be known, as in practice they might even be time-varying: this leads to the matrices $\mathbf{A}_{1\sigma}$ and $\mathbf{A}_{2\sigma}$ (positive definite for heavy-lift vessels [25]) being time-varying and uncertain. The following assumption highlights the nature of uncertainties considered in this work.

Assumption 1 (Uncertainty)**.** *Let $\mathbf{A}_{i\sigma}$'s be decomposable into two positive definite matrices $\hat{\mathbf{A}}_{i\sigma}$ (known nominal part) and $\tilde{\mathbf{A}}_{i\sigma}$ (unknown perturbation) such that $\mathbf{A}_{i\sigma}(t) = \hat{\mathbf{A}}_{i\sigma} + \tilde{\mathbf{A}}_{i\sigma}(t)$. Let $\Delta\mathbf{A}_{i\sigma}$ be the maximum possible perturbation*

[1]As offshore heavy-lift vessels are quite large in size including the payload, variation in mass and inertia parameters are usually negligible [25]

ranges such that $||\tilde{\mathbf{A}}_{i\sigma}(t)|| \leq ||\Delta\mathbf{A}_{i\sigma}|| \ \forall t$. *The knowledge of* $\hat{\mathbf{A}}_{i\sigma}$ *and* $\Delta\mathbf{A}_{i\sigma}$ *is available for control design.*

Control Objective: Without loss of generality we consider the desired position to be zero, i.e. the DP should keep $\boldsymbol{\eta}$ close to $\mathbf{0}$. The objective is to develop a switched control $\boldsymbol{\tau}_\sigma$ for the switched heavy-lift vessel dynamics (4) that can handle the complete offshore construction scenario of Fig. 1 while coping with the uncertainty outlined in Assumption 1.

III. Controller Design and Analysis

Observer-based control is very common in DP as a way to filter high-frequency environmental disturbances and measurement noises [24], [31]. Motivated by this common practice, an observer-based switched robust controller[2] is designed as

$$\dot{\hat{\boldsymbol{\eta}}} = \mathbf{J}\hat{\boldsymbol{\nu}} - \mathbf{K}_\sigma\hat{\boldsymbol{\eta}} + \mathbf{K}_{1\sigma}\tilde{\boldsymbol{\eta}}, \tag{9}$$

$$\dot{\hat{\boldsymbol{\nu}}} = -\hat{\mathbf{A}}_{1\sigma}\hat{\boldsymbol{\eta}} - \hat{\mathbf{A}}_{2\sigma}\hat{\boldsymbol{\nu}} + \mathbf{M}_\sigma^{-1}\boldsymbol{\tau}_\sigma + \mathbf{K}_{2\sigma}\hat{\boldsymbol{\eta}}, \tag{10}$$

$$\begin{aligned}\boldsymbol{\tau}_\sigma = \mathbf{M}_\sigma\{&(\hat{\mathbf{A}}_{1\sigma} - \mathbf{K}_{2\sigma} - \mathbf{P}_{4\sigma}^{-1}\mathbf{J}^T\mathbf{P}_{3\sigma})\hat{\boldsymbol{\eta}} \\ &+ (\hat{\mathbf{A}}_{2\sigma} - (\rho_\sigma + \rho_{1\sigma}))\hat{\boldsymbol{\nu}}\},\end{aligned} \tag{11}$$

where $\mathbf{J}(\psi)$ is written as $\mathbf{J}$ for compactness; $\hat{\boldsymbol{\eta}}$ and $\hat{\boldsymbol{\nu}}$ are the observations of $\boldsymbol{\eta}$ and $\boldsymbol{\nu}$ respectively, and $\tilde{\boldsymbol{\eta}} \triangleq \boldsymbol{\eta} - \hat{\boldsymbol{\eta}}$, $\tilde{\boldsymbol{\nu}} \triangleq \boldsymbol{\nu} - \hat{\boldsymbol{\nu}}$ are the corresponding observer errors. The various dynamics parameters and variables are given in Table II.

The observer dynamics (9)-(10) are constructed based on (3)-(4) with available system knowledge from Assumption 1. The observer and control gains $\mathbf{H}_\sigma, \mathbf{K}_\sigma, \mathbf{K}_{1\sigma}, \mathbf{K}_{2\sigma}, \rho_{1\sigma}, \rho_\sigma$ and $\mathbf{P}_{i\sigma}$ in (9)-(11) are used for system stability and robustness against uncertainties, and are designed as

$$\begin{aligned}\lambda_{\min}(\mathbf{P}_{1\sigma}\mathbf{K}_{1\sigma}) > ||&(1/2\beta)(\Delta\mathbf{A}_{1\sigma} - \mathbf{K}_{2\sigma})^T\mathbf{P}_{2\sigma}\mathbf{H}_\sigma^{-1}\mathbf{P}_{2\sigma} \\ &\times (\Delta\mathbf{A}_{1\sigma} - \mathbf{K}_{2\sigma})||,\end{aligned} \tag{12}$$

$$\begin{aligned}\lambda_{\min}(\mathbf{P}_{3\sigma}\mathbf{K}_\sigma) > ||&(1/2\beta)(\Delta\mathbf{A}_{1\sigma} + \mathbf{K}_{2\sigma})^T\mathbf{P}_{2\sigma}\mathbf{H}_\sigma^{-1}\mathbf{P}_{2\sigma} \\ &\times (\Delta\mathbf{A}_{1\sigma} + \mathbf{K}_{2\sigma})||,\end{aligned} \tag{13}$$

$$\begin{aligned}\lambda_{\min}(\mathbf{P}_{4\sigma})\rho_\sigma > ||&(1/2\beta)\Delta\mathbf{A}_{2\sigma}^T\mathbf{P}_{2\sigma}\mathbf{H}_\sigma^{-1}\mathbf{P}_{2\sigma}\Delta\mathbf{A}_{2\sigma}|| \\ &+ ||\Delta\mathbf{d}_\sigma||,\end{aligned} \tag{14}$$

$$\rho_{1\sigma} = \alpha\int_0^t ||(\mathbf{K}_{1\sigma} + \mathbf{K}_\sigma)||||\hat{\boldsymbol{\eta}}(\varpi)||||\tilde{\boldsymbol{\eta}}(\varpi)||\mathrm{d}\varpi, \tag{15}$$

$$\mathbf{K}_{2\sigma}(t) = -\hat{\mathbf{A}}_{1\sigma} + \mathbf{J}^T(t), \tag{16}$$

$$\lambda_{\min}(\mathbf{P}_{2\sigma}\hat{\mathbf{A}}_{2\sigma}) > ||(3\beta/2)\mathbf{H}_\sigma||. \tag{17}$$

where $\alpha > 1$ and $\beta > 0$ are design scalars.

Remark 2 (Selection of gains)**.** *According to Assumption 1,* $\hat{\mathbf{A}}_{2\sigma}$ *is the nominal knowledge of* $\mathbf{A}_{2\sigma}$*. Therefore, (17) provides a selection criterion for* $\beta, \mathbf{H}_\sigma$ *and* $\mathbf{P}_{2\sigma}$*, which in turn guide the section of* $\mathbf{P}_{1\sigma}, \mathbf{P}_{3\sigma}, \mathbf{P}_{4\sigma}, \mathbf{K}_{1\sigma}, \mathbf{K}_\sigma, \rho_\sigma$ *and* $\rho_{1\sigma}$ *via (12), (13), (14) and (15).*

Let us define

$$\mathbf{P}_\sigma \triangleq diag\{\mathbf{P}_{1\sigma}, \mathbf{P}_{2\sigma}, \mathbf{P}_{3\sigma}, \mathbf{P}_{4\sigma}\}, \tag{18}$$

$$\varrho_M \triangleq \max_{\sigma\in\Omega}\lambda_{\max}(\mathbf{P}_\sigma), \ \varrho_m \triangleq \min_{\sigma\in\Omega}\lambda_{\min}(\mathbf{P}_\sigma), \tag{19}$$

$$\kappa \triangleq 2\min_{\sigma\in\Omega}\min_{i=1,\cdots,4}(\lambda_{\min}(\mathbf{Q}_{i\sigma}))/\varrho_M, \tag{20}$$

[2]From now on, the time index t will be omitted whenever unambiguous.

Table II: System Parameters and Variables

Variables	
$\boldsymbol{\eta} = [x, y, \psi]^T$	Vessel position and yaw angle
$\hat{\boldsymbol{\eta}}$	Filtered observation of $\boldsymbol{\eta}$
$\tilde{\boldsymbol{\eta}}$	Observation error $\boldsymbol{\eta} - \hat{\boldsymbol{\eta}}$
$\mathbf{J}(\psi)$	Rotation matrix from vessel's body to NED frame
$\boldsymbol{\nu} = [u, v, r]^T$	Vessel velocity and angular velocity
$\hat{\boldsymbol{\nu}}$	Filtered observation of $\boldsymbol{\nu}$
$\tilde{\boldsymbol{\nu}}$	Observation error $\boldsymbol{\nu} - \hat{\boldsymbol{\nu}}$
$\sigma \in \{1, 2, 3\}$	Construction phase (i.e. mode)
$\boldsymbol{\tau}_c$	Force from crane winch (during mooring mode)
$\boldsymbol{\tau}_l$	Force from load (during free-hanging mode)
$\boldsymbol{\tau}$	Control input
$\bar{\mathbf{d}}$	Bounded environmental disturbances
$\mathbf{F}_\sigma$	Mooring stiffness in mode σ
$\boldsymbol{\tau}_{l\sigma}$	Force from hanging of the load in mode σ
Parameters	
$\mathbf{M}$	Mass matrix of the vessel in 3 DoFs
$\mathbf{D}$	Damping matrix of the vessel in 3 DoFs
$\mathbf{M}_\sigma$	Mass matrix of the vessel in mode σ
$\hat{\mathbf{A}}_{i\sigma}$	Nominal part of $\mathbf{A}_{i\sigma}$
$\triangle\mathbf{A}_{i\sigma}$	Maximum possible perturbation ranges
Perturbations terms (unknown to designer)	
$\tilde{\mathbf{A}}_{i\sigma}$	Bounded unknown part of $\mathbf{A}_{i\sigma}$

where $\mathbf{Q}_{i\sigma}$ are positive definite matrices defined as

$$\begin{aligned}\mathbf{Q}_{1\sigma} &\triangleq \{\mathbf{P}_{1\sigma}\mathbf{K}_{1\sigma} - (1/2\beta)(\Delta\mathbf{A}_{1\sigma} - \mathbf{K}_{2\sigma})^T\mathbf{P}_{2\sigma}\mathbf{H}_\sigma^{-1}\mathbf{P}_{2\sigma}\times \\ &\qquad \times (\Delta\mathbf{A}_{1\sigma} - \mathbf{K}_{2\sigma})\}, \\ \mathbf{Q}_{2\sigma} &\triangleq \{\mathbf{P}_{2\sigma}\hat{\mathbf{A}}_{2\sigma} - ((3\beta/2)\mathbf{H}_\sigma)\}, \\ \mathbf{Q}_{3\sigma} &\triangleq \{\mathbf{P}_{3\sigma}\mathbf{K}_\sigma - (1/2\beta)(\Delta\mathbf{A}_{1\sigma} + \mathbf{K}_{2\sigma})^T\mathbf{P}_{2\sigma}\mathbf{H}_\sigma^{-1}\mathbf{P}_{2\sigma}\times \\ &\qquad \times (\Delta\mathbf{A}_{1\sigma} + \mathbf{K}_{2\sigma})\}, \\ \mathbf{Q}_{4\sigma} &\triangleq \{\rho_\sigma\mathbf{P}_{4\sigma} - (1/2\beta)\Delta\mathbf{A}_{2\sigma}^T\mathbf{P}_{2\sigma}\mathbf{H}_\sigma^{-1}\mathbf{P}_{2\sigma}\Delta\mathbf{A}_{2\sigma}\}.\end{aligned}$$

Following Definition 1, let us consider the switching signal $\sigma(\cdot)$ with an average dwell time ϑ satisfying

$$\vartheta > \vartheta^* = \ln\mu/\zeta, \tag{21}$$

where $\mu \triangleq \varrho_M/\varrho_m$ and $0 < \zeta < \kappa$.

Remark 3 (Continuity of the states)**.** *At switching instants, the control/observer gains* $\mathbf{H}_\sigma, \mathbf{K}_\sigma, \mathbf{K}_{1\sigma}, \mathbf{K}_{2\sigma}, \rho_{1\sigma}, \rho_\sigma$ *and* $\mathbf{P}_{i\sigma}$ *are designed to switch accordingly, i.e. to change discontinuously to handle the new phase: however, it must be noticed that the states* $\boldsymbol{\eta}, \boldsymbol{\nu}$ *in (3)-(4) and their observed values* $\hat{\boldsymbol{\eta}}, \hat{\boldsymbol{\nu}}$ *in (9)-(10) remain continuous despite switching. Therefore, issues of chattering as in state-dependent switching (sliding mode) will be absent in ADT time-driven switching [27].*

Remark 4 (Co-design of switching and control law)**.** *In switching control literature it is well known that stability cannot be achieved for arbitrarily switching signals [28], [30], [32]. This implies that one should not only design a stabilizing control law, but also a stabilizing family of switching laws. In the proposed DP setting, the switched controller is (9)-(11), whereas the switching signal is given by (21) in the ADT framework of Definition 1. The parameter in (21) should be properly tuned so that* ϑ^* *represents the typical duration of the different construction phases (cf. Remark 1).*

The closed-loop system stability is analyzed using the following Lyapunov function:

$$V(\boldsymbol{\xi}) = V_1(\tilde{\boldsymbol{\eta}}, \tilde{\boldsymbol{\nu}}) + V_2(\hat{\boldsymbol{\eta}}, \hat{\boldsymbol{\nu}}) = \frac{1}{2}\boldsymbol{\xi}^T \mathbf{P}_\sigma \boldsymbol{\xi}, \tag{22}$$

where $\boldsymbol{\xi} \triangleq [\tilde{\boldsymbol{\eta}}^T \ \tilde{\boldsymbol{\nu}}^T \ \hat{\boldsymbol{\eta}}^T \ \hat{\boldsymbol{\nu}}^T]^T$ and

$$V_1 \triangleq \frac{1}{2}(\tilde{\boldsymbol{\eta}}^T \mathbf{P}_{1\sigma} \tilde{\boldsymbol{\eta}} + \tilde{\boldsymbol{\nu}}^T \mathbf{P}_{2\sigma} \tilde{\boldsymbol{\nu}}),$$
$$V_2 \triangleq \frac{1}{2}(\hat{\boldsymbol{\eta}}^T \mathbf{P}_{3\sigma} \hat{\boldsymbol{\eta}} + \hat{\boldsymbol{\nu}}^T \mathbf{P}_{4\sigma} \hat{\boldsymbol{\nu}}).$$

The following theorem states the closed-loop system stability:

Theorem 1. *Under Assumption 1, the switched system (3)-(4) employing the switched control input law (9)-(11) and satisfying the gain selection criteria (12)-(17) is Globally Uniformly Ultimately Bounded (GUUB) for any ADT switching signal satisfying (21). This implies*

$$V(t) \leq \max\left\{bV(t_0), b\mu\mathcal{B}\right\}, \quad \forall t \geq t_0. \tag{23}$$

where $b \triangleq \exp\left(N_0 \ln \mu\right)$, $\mathcal{B} \triangleq \max_\sigma \left(\dfrac{2||\Delta \mathbf{d}_\sigma||^2}{\varrho_m(\kappa - \zeta)^2}, \dfrac{\varrho_m}{2\alpha} \right)$.

Proof. See Appendix. □

Overall Control Structure: Summarizing, the proposed control law and switching law comprise of the design steps as enumerated in Algorithm 1.

Algorithm 1 Design steps of the proposed switched controller

Step 1 (preliminary gains): design suitable matrices $\mathbf{H}_\sigma, \mathbf{P}_{2\sigma}$ such that (17) is satisfied for user-defined positive scalar β;
Step 2 (observer and control gains): based on the results from Step 1, design $\mathbf{P}_{1\sigma}, \mathbf{P}_{3\sigma}, \mathbf{P}_{4\sigma}, \mathbf{K}_{1\sigma}, \mathbf{K}_\sigma, \rho_\sigma$ and $\rho_{1\sigma}$ via (12), (13), (14) and (15);
Step 3 (ADT gains): compute the gains ϱ_M, ϱ_m, and κ as in (18)-(20);
Step 4 (observer based robust law): the observer is as in (9)-(10) with control input $\boldsymbol{\tau}_\sigma$ according to (11);
Step 5 (switching law): the system can change dynamics according to any ADT switching law satisfying (21) resulting from Step 4.

Key Performance Indicators: From (23), upper bounds on the position error $\boldsymbol{\eta}$ and control input $\boldsymbol{\tau}$ can be computed. These bounds can serve the purpose of key performance indicators (KPIs).

Utilizing the relations $V \geq (\varrho_m/2)||\boldsymbol{\xi}||^2 \geq (\varrho_m/2)||\hat{\boldsymbol{\eta}}||^2$ and $V \geq (\varrho_m/2)||\boldsymbol{\xi}||^2 \geq (\varrho_m/2)||\tilde{\boldsymbol{\eta}}||^2$, the upper bound on $\boldsymbol{\eta}$ can be computed as follows:

$$\begin{aligned} ||\boldsymbol{\eta}|| &= ||\tilde{\boldsymbol{\eta}} + \hat{\boldsymbol{\eta}}|| \leq 2\sqrt{2V/\varrho_m} \\ &\leq 2\sqrt{(2/\varrho_m)\max\left\{bV(t_0), b\mu\mathcal{B}\right\}} \triangleq 2\bar{\mathcal{B}}. \end{aligned} \tag{24}$$

Similarly, an upper bound on $\boldsymbol{\tau}_\sigma$ can be derived from (11) as

$$\begin{aligned} ||\boldsymbol{\tau}_\sigma|| &= ||\mathbf{M}_\sigma\{(\hat{\mathbf{A}}_{1\sigma} - \mathbf{K}_{2\sigma} - \mathbf{P}_{4\sigma}^{-1}\mathbf{J}^T\mathbf{P}_{3\sigma})\hat{\boldsymbol{\eta}} \\ &\quad + (\hat{\mathbf{A}}_{2\sigma} - (\rho_\sigma + \rho_{1\sigma}))\hat{\boldsymbol{\nu}}\}|| \\ &\leq \bar{\mathcal{B}}||\mathbf{M}_\sigma||\{||(\hat{\mathbf{A}}_{1\sigma} - \mathbf{K}_{2\sigma} - \mathbf{P}_{4\sigma}^{-1}\mathbf{J}^T\mathbf{P}_{3\sigma})|| \\ &\quad + ||(\hat{\mathbf{A}}_{2\sigma} - (\rho_\sigma + \rho_{1\sigma}))||\}. \end{aligned} \tag{25}$$

Remark 5 (Phase-dependent tuning)**.** *The control bounds in (25) are different for each phase, i.e. one can tune the gains in (12)-(17) independently for each phase. On the other hand, a single non-switched controller tuned only for one of the three phases might result in a too shallow/too aggressive control in the other phases (cf. simulations in the following section).*

IV. Simulation Results and Analysis

Though DP controllers are conventionally designed for three DoFs dynamics, their performance should be properly verified on realistic six DoFs dynamics [24], [26]. Therefore, in this section we verify the proposed controller on a six DoFs simulation platform, based on the S-175 model from MSS toolbox [33] with vessel dynamics generated by WAMIT.

A. Simulation Model

Extending the approach in [25] to a switched framework, the six DoFs heavy-lift vessel's dynamics can be expressed as

$$\dot{\overline{\boldsymbol{\eta}}} = \overline{\mathbf{J}}(\phi, \theta, \psi)\overline{\boldsymbol{\nu}}, \tag{26}$$

$$\begin{aligned} \overline{\mathbf{M}}_\sigma\dot{\overline{\boldsymbol{\nu}}} + \overline{\mathbf{D}}\overline{\boldsymbol{\nu}} + \overline{\mathbf{C}}(\overline{\boldsymbol{\nu}})\overline{\boldsymbol{\nu}}(t) + \overline{\mathbf{G}}(\overline{\boldsymbol{\eta}}) + \overline{\mathbf{g}}_\sigma \\ = \boldsymbol{\tau}_{th} + \boldsymbol{\tau}_e + \boldsymbol{\tau}_{c\sigma} + \boldsymbol{\tau}_{l\sigma}, \end{aligned} \tag{27}$$

where $\overline{\boldsymbol{\nu}} = [u, v, w, p, q, r]^T$ is the vessel's velocity in body-fixed coordinates; $\overline{\boldsymbol{\eta}} = [x, y, z, \phi, \theta, \psi]^T$ is the vessel position in North-East-Down (NED) coordinates; $\overline{\mathbf{J}}(\phi, \theta, \psi) \in \mathbb{R}^{6\times6}$ is the transformation matrix from body-fixed to NED coordinates; $\boldsymbol{\tau}_{th} \in \mathbb{R}^6$ comprises forces and moments by the propulsion system; $\boldsymbol{\tau}_e \in \mathbb{R}^6$ denotes forces and moments induced by currents, wind and waves; $\overline{\mathbf{M}}_\sigma \in \mathbb{R}^{6\times6}$ is the mass matrix of the vessel; $\overline{\mathbf{D}} \in \mathbb{R}^{6\times6}$ is the damping matrix; $\overline{\mathbf{C}} \in \mathbb{R}^{6\times6}$ is the Coriolis matrix; $\overline{\mathbf{g}}_\sigma = [0, 0, -M_{v\sigma}g, 0, 0, 0]^T$ is the gravity vector on the vessel, $M_{v\sigma}$ being the vessel mass and g the gravity acceleration; $\overline{\mathbf{G}}(\overline{\boldsymbol{\eta}})$ represents the hydrostatic force on the vessel. We assume that the force in the crane wires is controlled by a crane winch during the mooring mode, and the initial length of the elastic crane wires is fixed when the load is fully lifted (i.e. when the system is in free-hanging mode), then the crane force can be expressed as a combination of $\boldsymbol{\tau}_{c\sigma}$ and $\boldsymbol{\tau}_{l\sigma}$, where $\boldsymbol{\tau}_{c\sigma} = [\mathbf{F}_{c\sigma}, \mathbf{T}_{c\sigma}]^T$ and $\boldsymbol{\tau}_{l\sigma} = [\mathbf{F}_{l\sigma}, \mathbf{T}_{l\sigma}]^T$ contain forces and moments from the crane and load.

Similarly to the 3 DoF case, the 6 DoF dynamics are modelled in a switched framework (cf. Fig. 2 and Table III):

Phase 1: No Load Load and crane do not act on the vessel; the environmental forces/moments are the only external action.

Phase 2: Mooring Mode The load does not contribute any force/moment, but the lifting (or dropping) of the crane causes a force and a moment by hydraulic winch modelled as:

$$\mathbf{F}_{c\sigma} = F_h \frac{\boldsymbol{\delta}_l}{||\boldsymbol{\delta}_l||}, \ \mathbf{T}_{c\sigma} = \mathbf{r}_{ct} \times \mathbf{F}_{c\sigma} \tag{28}$$

where F_h is the tension in the crane wires; $\boldsymbol{\delta}_l = \mathbf{p}_{ct} - \mathbf{J}_3^T(\phi, \theta, \psi)\boldsymbol{\eta}_l$, with $\mathbf{p}_{ct}$ being the time-independent position of the crane-tip, $\mathbf{J}_3$ the rotation matrix from body-fixed frame to NED in 3 DoFs, and $\boldsymbol{\eta}_l$ the load position in NED (constant during mooring); $\mathbf{r}_{ct} \in \mathbb{R}^3$ is the vector from vessel's Center of Rotation to the crane tip.

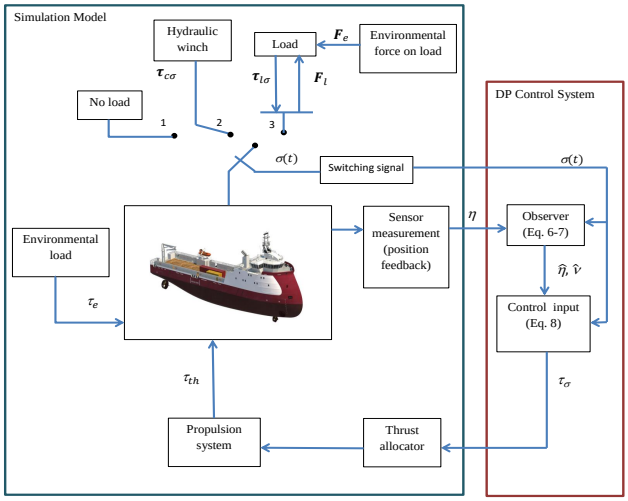

Figure 2: Heavy-lift vessel during construction. In Phase 1 there is no crane/load force; in Phase 2 the crane force is determined by the hydraulic winch; in Phase 3 the load force is modeled as a spring/damper system.

Phase 3: Free-hanging Mode No external contribution from the crane occurs, while the force and moment induced by the load can be expressed as:

$$\mathbf{F}_{l\sigma} = \begin{cases} (K_w\tilde{\delta}' + D_w\dot{\tilde{\delta}}')\frac{\boldsymbol{\delta}_l}{||\boldsymbol{\delta}_l||}, & \text{if } \tilde{\delta}' > 0; \\ 0, & \text{if } \tilde{\delta}' \leq 0. \end{cases}, \quad \mathbf{T}_{l\sigma} = \mathbf{r}_{ct} \times \mathbf{F}_{l\sigma}, \tag{29}$$

where $\tilde{\delta}'(t)$ is the elastic elongation of the crane wires and $\boldsymbol{\delta}_l$ is similar to Phase 2, but the load position $\boldsymbol{\eta}_l$ is not constant, but with its own 3DoF dynamics

$$\mathbf{M}_l\ddot{\boldsymbol{\eta}}_l + \mathbf{D}_l\dot{\boldsymbol{\eta}}_l + \mathbf{g}_l + \mathbf{F}_b = \mathbf{F}_e - \mathbf{J}_3(\phi,\theta,\psi)\mathbf{F}_{l\sigma}, \tag{30}$$

where $\mathbf{M}_l \in \mathbb{R}^{3\times3}$ is the mass matrix of the load, $\mathbf{D}_l \in \mathbb{R}^{3\times3}$ is the damping matrix of the load, $\mathbf{F}_b$ is the buoyancy force, $\mathbf{F}_e$ is the environmental force on the load.

Details of other subsystems on board of the heavy-lift vessel, i.e. thrust allocator, and propulsion systems are not reported for lack of space, but can be found in [26].

B. Design Parameters

The following design parameters have been used:

$$\hat{\mathbf{A}}_{11} = \begin{bmatrix} 2.7\cdot10^{-5} & 0 & 0 \\ 0 & 2.1\cdot10^{-5} & -4.2\cdot10^{-9} \\ 0 & -4.2\cdot10^{-9} & 1.1\cdot10^{-8} \end{bmatrix},$$

$$\hat{\mathbf{A}}_{12} = \begin{bmatrix} 1.6\cdot10^{-3} & 0 & 0 \\ 0 & 1.2\cdot10^{-3} & -2.5\cdot10^{-7} \\ 0 & -2.5\cdot10^{-7} & 6.3\cdot10^{-7} \end{bmatrix},$$

$$\hat{\mathbf{A}}_{13} = \begin{bmatrix} 2.7\cdot10^{-4} & 0 & 0 \\ 0 & 2.1\cdot10^{-4} & -4.2\cdot10^{-8} \\ 0 & -4.2\cdot10^{-8} & 1.1\cdot10^{-7} \end{bmatrix},$$

$$\Delta\mathbf{A}_{11} = 0.4\hat{\mathbf{A}}_{11}, \Delta\mathbf{A}_{12} = 0.9\hat{\mathbf{A}}_{12}, \Delta\mathbf{A}_{13} = \hat{\mathbf{A}}_{13}$$

Table III: Forces and Moments during the Three Construction Phases

Phase 1 ($\sigma = 1$)	$\boldsymbol{\tau}_{l\sigma} = \mathbf{0},\ \boldsymbol{\tau}_{c\sigma} = \mathbf{0},$
Phase 2 ($\sigma = 2$)	$\boldsymbol{\tau}_{l\sigma} = \mathbf{0},\ \mathbf{F}_{c\sigma} = F_h\frac{\boldsymbol{\delta}_l}{\|\|\boldsymbol{\delta}_l\|\|}, \mathbf{T}_{c\sigma} = \mathbf{r}_{ct} \times \mathbf{F}_{c\sigma}$
Phase 3 ($\sigma = 3$)	$\mathbf{F}_{l\sigma} = \begin{cases} (K_w\tilde{\delta}' + D_w\dot{\tilde{\delta}}')\frac{\boldsymbol{\delta}_l}{\|\|\boldsymbol{\delta}_l\|\|}, & \text{if } \tilde{\delta}' > 0; \\ 0, & \text{if } \tilde{\delta}' \leq 0, \end{cases}$ $\mathbf{T}_{l\sigma} = \mathbf{r}_{ct} \times \mathbf{F}_{l\sigma}, \boldsymbol{\tau}_{c\sigma} = \mathbf{0}$

Table IV: Parameters for Environmental Forces/Moments

Current Velocity	Wind Velocity	Significant Wave Height	Mean Wind and Wave Angle
$[u_c, v_c] = [0.5, 0.3]m/s$	$2.5m/s$	$0.5m$	$210°$

$$\hat{\mathbf{A}}_{21} = \hat{\mathbf{A}}_{22} = \hat{\mathbf{A}}_{23} = \begin{bmatrix} 1.8\cdot10^{-2} & 0 & 0 \\ 0 & 1.2\cdot10^{-1} & -6.3\cdot10^{-2} \\ 0 & 2.7\cdot10^{-5} & 1.4\cdot10^{-1} \end{bmatrix},$$

$$\Delta\mathbf{A}_{21} = \Delta\mathbf{A}_{22} = \Delta\mathbf{A}_{23} = 0.2\hat{\mathbf{A}}_{21},$$
$$\mathbf{P}_{21} = \mathbf{I},\ \mathbf{P}_{11} = \mathbf{P}_{31} = \mathbf{P}_{41} = 10\mathbf{P}_{21},$$
$$\mathbf{P}_{22} = 2\mathbf{I},\ \mathbf{P}_{12} = \mathbf{P}_{32} = \mathbf{P}_{42} = 10\mathbf{P}_{22},$$
$$\mathbf{P}_{23} = 1.5\mathbf{I},\ \mathbf{P}_{13} = \mathbf{P}_{33} = \mathbf{P}_{43} = 10\mathbf{P}_{23},$$
$$\mathbf{H}_1 = 1.1\cdot10^{-3}\mathbf{I}, \mathbf{H}_2 = 2.2\cdot10^{-3}\mathbf{I}, \mathbf{H}_3 = 1.7\cdot10^{-3}\mathbf{I},$$
$$\mathbf{K}_1 = 4.57\mathbf{I}, \mathbf{K}_2 = 4.57\mathbf{I}, \mathbf{K}_3 = 4.57\mathbf{I},$$
$$\mathbf{K}_{11} = 4.57\mathbf{I}, \mathbf{K}_{12} = 4.61\mathbf{I}, \mathbf{K}_{13} = 4.58\mathbf{I},$$
$$\rho_1 = 1.53, \rho_2 = 1.55, \rho_3 = 1.54, \alpha = 2, \beta = 1.$$

where the nominal value of $\mathbf{A}_{1\sigma}$ and $\mathbf{A}_{2\sigma}$ have been chosen based on the nominal knowledge of load, vessel's mass and damping matrix. The above gains and $\zeta = 0.9\kappa$ yields the ADT $\vartheta^* = 9.24$s according to (21).

C. Simulation Results

Simulations are carried out under the 'smooth-to-slight' sea-state with environmental conditions shown in Table IV. The following simulation scenario is considered:

Phase 1 ($\sigma = 1$) : $0s - 150s$;
Phase 2 ($\sigma = 2$) : $150s - 750s$;
Phase 3 ($\sigma = 3$) : $750s - 900s$.

The performance of the proposed controller is shown in Figs. 3 and 4. To further demonstrate the effectiveness and importance of the proposed switched design, we formulate a non-switched controller by applying the control gains in (9)-(11) for $\sigma = 2$ to all three phases. Performance of this non-switched design is shown in Figs. 5 and 6, and are collected in Table V in terms of root-mean-squared error (RMSE) and maximum offset of the vessel from the desired set-point. It is crucial to notice that the non-switched controller causes significant position offset and large oscillations (especially in the surge direction), which could cause collision between the platform and the vessel. Such oscillations confirm some reported real-life hazardous scenarios (cf. Fig. 1.2 in [6]), and the necessity for switching control.

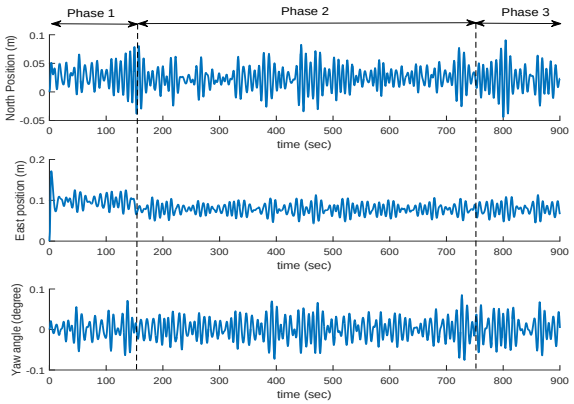

Figure 3: Vessel position under switched control

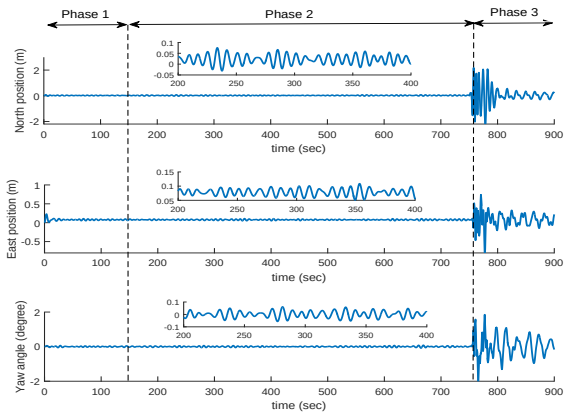

Figure 5: Vessel position under non-switched control

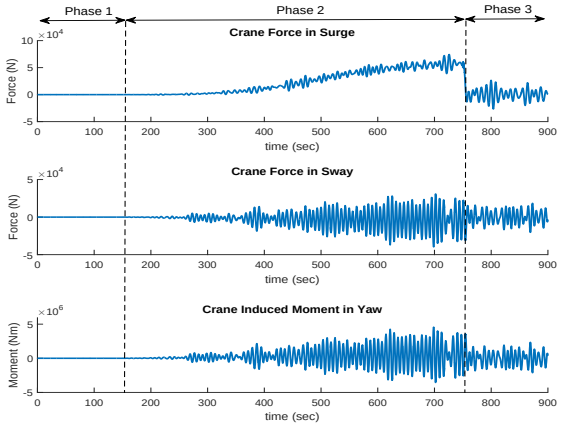

Figure 4: Crane force under switched control

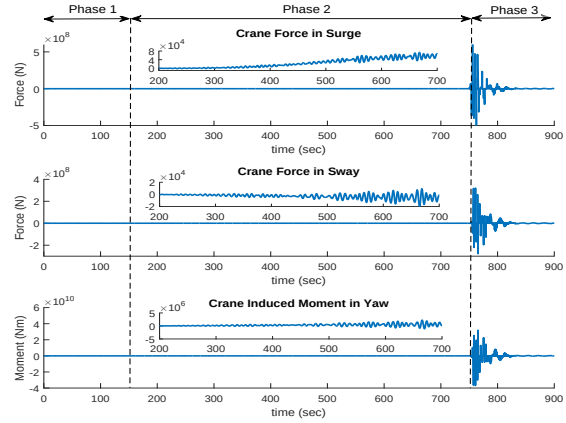

Figure 6: Crane force under non-switched control

Table V: Performance Comparison of the Proposed Switched Controller and Non-switched Controller

		Proposed Switched Controller			Non-switched Controller		
Phase		1	2	3	1	2	3
RMSE [m]	North	0.03	0.03	0.03	0.03	0.03	0.65
	East	0.1	0.08	0.08	0.08	0.08	0.20
	Yaw	0.02	0.03	0.03	0.02	0.03	0.60
Maximum Offset [m]	North	0.08	0.08	0.09	0.08	0.08	2.32
	East	0.17	0.11	0.11	0.23	0.11	0.85
	Yaw	0.07	0.09	0.07	0.06	0.08	2.21

V. Conclusions and Future Work

In this work, a switched controller was proposed for the first time to tackle the interchanging dynamics arising during a complete construction operation of a heavy-lift offshore vessel. The proposed control framework was studied analytically and its effectiveness was verified in simulation via a realistic model of heavy-lift vessel. The simulations show that the proposed solution can effectively avert an otherwise operational hazard.

In this work the switching time is determined using human input. Further work could focus on autonomously switching the controller by identifying the different construction phases from real-time measurements.

Appendix

In view of the disturbances, the stability notion used in thus work is the so-called Globally Uniformly Ultimately Bounded (GUUB) stability, as formalized by the following definition:

Definition 2 (GUUB [34])**.** *System (3)-(4) is GUUB if there exists a convex and compact set Υ such that for every initial condition $(\boldsymbol{\eta}(0), \boldsymbol{\nu}(0))$, there exists a finite $T(\boldsymbol{\eta}(0), \boldsymbol{\nu}(0))$ such that $(\boldsymbol{\eta}(t), \boldsymbol{\nu}(t)) \in \Upsilon$ for all $t \geq T(\boldsymbol{\eta}(0), \boldsymbol{\nu}(0))$.*

Proof of Theorem 1: Using (3), (4), (9) and (10), the observer error dynamics can be formulated as

$$\dot{\tilde{\boldsymbol{\eta}}} = \dot{\boldsymbol{\eta}} - \dot{\hat{\boldsymbol{\eta}}} = \mathbf{J}\tilde{\boldsymbol{\nu}} + \mathbf{K}_\sigma \hat{\boldsymbol{\eta}} - \mathbf{K}_{1\sigma}\tilde{\boldsymbol{\eta}}, \tag{31}$$

$$\dot{\tilde{\boldsymbol{\nu}}} = \dot{\boldsymbol{\nu}} - \dot{\hat{\boldsymbol{\nu}}} = -\hat{\mathbf{A}}_{1\sigma}\tilde{\boldsymbol{\eta}} - \tilde{\mathbf{A}}_{1\sigma}(\tilde{\boldsymbol{\eta}} + \hat{\boldsymbol{\eta}}) - \mathbf{K}_{2\sigma}\hat{\boldsymbol{\eta}} - \hat{\mathbf{A}}_{2\sigma}\tilde{\boldsymbol{\nu}} - \tilde{\mathbf{A}}_{2\sigma}(\tilde{\boldsymbol{\nu}} + \hat{\boldsymbol{\nu}}) + \mathbf{d}_\sigma. \tag{32}$$

The Lyapunov function $V(\cdot)$ is continuous in between switching instants but, due to switching to different $\mathbf{P}_\sigma$, it might be discontinuous at switching instants. The behaviour of the Lyapunov function is studied at $t_{l+1},\ l \in \mathbb{N}^+$. Let the active subsystem be $\sigma(t_{l+1}^-)$ when $t \in [t_l \quad t_{l+1})$ and $\sigma(t_{l+1})$ when $t \in [t_{l+1} \quad t_{l+2})$. We have before and after switching

$$V(t_{l+1}^-) = (1/2)\boldsymbol{\xi}^T(t_{l+1}^-)\mathbf{P}_{\sigma(t_{l+1}^-)}\boldsymbol{\xi}(t_{l+1}^-)$$

$$V(t_{l+1}) = (1/2)\boldsymbol{\xi}^T(t_{l+1})\mathbf{P}_{\sigma(t_{l+1})}\boldsymbol{\xi}(t_{l+1}),$$

respectively. Thanks to the continuity of $\hat{\boldsymbol{\eta}}, \hat{\boldsymbol{\nu}}$ in (9)-(10) and of $\tilde{\boldsymbol{\eta}}, \tilde{\boldsymbol{\nu}}$ in (31)-(32) (cf. Remark 3) we have $\hat{\boldsymbol{\eta}}(t_{l+1}^-) = \hat{\boldsymbol{\eta}}(t_{l+1})$, $\hat{\boldsymbol{\nu}}(t_{l+1}^-) = \hat{\boldsymbol{\nu}}(t_{l+1})$, $\tilde{\boldsymbol{\eta}}(t_{l+1}^-) = \tilde{\boldsymbol{\eta}}(t_{l+1})$ and $\tilde{\boldsymbol{\nu}}(t_{l+1}^-) = \tilde{\boldsymbol{\nu}}(t_{l+1})$. This leads to $\boldsymbol{\xi}(t_{l+1}^-) = \boldsymbol{\xi}(t_{l+1})$. Further, owing to the facts $\boldsymbol{\xi}^T(t)\mathbf{P}_{\sigma(t)}\boldsymbol{\xi}(t) \leq \varrho_M \boldsymbol{\xi}^T(t)\boldsymbol{\xi}(t)$ and $\boldsymbol{\xi}^T(t)\mathbf{P}_{\sigma(t)}\boldsymbol{\xi}(t) \geq \varrho_m \boldsymbol{\xi}^T(t)\boldsymbol{\xi}(t)$, one has

$$V(t_{l+1}) - V(t_{l+1}^-) = \frac{1}{2}\boldsymbol{\xi}^T(t_{l+1})(\mathbf{P}_{\sigma(t_{l+1})} - \mathbf{P}_{\sigma(t_{l+1}^-)})\boldsymbol{\xi}(t_{l+1})$$
$$\leq \frac{\varrho_M - \varrho_m}{2\varrho_m}\boldsymbol{\xi}^T(t_{l+1})\mathbf{P}_{\sigma(t_{l+1}^-)}\boldsymbol{\xi}(t_{l+1}) \leq \frac{\varrho_M - \varrho_m}{\varrho_m}V(t_{l+1}^-)$$
$$\Rightarrow V(t_{l+1}) \leq \mu V(t_{l+1}^-), \tag{33}$$

with $\mu = \varrho_M/\varrho_m \geq 1$. At this point, the behaviour of $V(\cdot)$ between two consecutive switching instants, i.e., when $t \in [t_l \;\; t_{l+1})$ can be studied.

Utilizing (31)-(32), the following can be achieved

$$\begin{aligned}\dot{V}_1 =& \tilde{\boldsymbol{\eta}}^T\mathbf{P}_{1\sigma}(-\mathbf{K}_{1\sigma}\tilde{\boldsymbol{\eta}} + \mathbf{K}_\sigma\hat{\boldsymbol{\eta}} + \mathbf{J}\tilde{\boldsymbol{\nu}})\\ &- \tilde{\boldsymbol{\nu}}^T\mathbf{P}_{2\sigma}(\hat{\mathbf{A}}_{2\sigma} + \tilde{\mathbf{A}}_{2\sigma})\tilde{\boldsymbol{\nu}} - \tilde{\boldsymbol{\nu}}^T\mathbf{P}_{2\sigma}(\hat{\mathbf{A}}_{1\sigma} + \tilde{\mathbf{A}}_{1\sigma})\tilde{\boldsymbol{\eta}}\\ &- \tilde{\boldsymbol{\nu}}^T\mathbf{P}_{2\sigma}(\tilde{\mathbf{A}}_{1\sigma} + \mathbf{K}_{2\sigma})\hat{\boldsymbol{\eta}} - \tilde{\boldsymbol{\nu}}^T\mathbf{P}_{2\sigma}\tilde{\mathbf{A}}_{2\sigma}\hat{\boldsymbol{\nu}} + \tilde{\boldsymbol{\nu}}^T\mathbf{P}_{2\sigma}\mathbf{d}_\sigma\\ \leq& -\tilde{\boldsymbol{\eta}}^T\mathbf{P}_{1\sigma}\mathbf{K}_{1\sigma}\tilde{\boldsymbol{\eta}} - \tilde{\boldsymbol{\nu}}^T\mathbf{P}_{2\sigma}\hat{\mathbf{A}}_{2\sigma}\tilde{\boldsymbol{\nu}} + \tilde{\boldsymbol{\eta}}^T\mathbf{P}_{1\sigma}\mathbf{K}_\sigma\hat{\boldsymbol{\eta}}\\ &+ \tilde{\boldsymbol{\nu}}^T\mathbf{P}_{2\sigma}\mathbf{d}_\sigma - \tilde{\boldsymbol{\nu}}^T\mathbf{P}_{2\sigma}(\tilde{\mathbf{A}}_{1\sigma} + \mathbf{K}_{2\sigma})\hat{\boldsymbol{\eta}}\\ &- \tilde{\boldsymbol{\nu}}^T\mathbf{P}_{2\sigma}(\tilde{\mathbf{A}}_{1\sigma} - \mathbf{K}_{2\sigma})\tilde{\boldsymbol{\eta}} - \tilde{\boldsymbol{\nu}}^T\mathbf{P}_{2\sigma}\tilde{\mathbf{A}}_{2\sigma}\hat{\boldsymbol{\nu}}.\end{aligned} \tag{34}$$

Further, using (9)-(11), the following can be deduced

$$\begin{aligned}\dot{V}_2 =& \hat{\boldsymbol{\eta}}^T\mathbf{P}_{3\sigma}(-\mathbf{K}_\sigma\hat{\boldsymbol{\eta}} + \mathbf{K}_{1\sigma}\tilde{\boldsymbol{\eta}} + \mathbf{J}\hat{\boldsymbol{\nu}})\\ &+ \hat{\boldsymbol{\nu}}^T\mathbf{P}_{4\sigma}(-(\rho_\sigma + \rho_{1\sigma})\hat{\boldsymbol{\nu}} - \mathbf{P}_{4\sigma}^{-1}\mathbf{J}^T\mathbf{P}_{3\sigma}\hat{\boldsymbol{\eta}})\\ =& -\hat{\boldsymbol{\eta}}^T\mathbf{P}_{3\sigma}\mathbf{K}_\sigma\hat{\boldsymbol{\eta}} - (\rho_\sigma + \rho_{1\sigma})\hat{\boldsymbol{\nu}}^T\mathbf{P}_{4\sigma}\hat{\boldsymbol{\nu}} + \tilde{\boldsymbol{\eta}}^T\mathbf{K}_{1\sigma}\mathbf{P}_{3\sigma}\hat{\boldsymbol{\eta}}.\end{aligned} \tag{35}$$

Given any scalar $\beta > 0$ and a positive definite matrix $\mathbf{H}_\sigma$, the following holds for any two non-zero vectors $\mathbf{z}$ and $\mathbf{z}_1$,

$$\pm 2\mathbf{z}^T\mathbf{z}_1 \leq \beta\mathbf{z}^T\mathbf{H}_\sigma\mathbf{z} + (1/\beta)\mathbf{z}_1^T\mathbf{H}_\sigma^{-1}\mathbf{z}_1. \tag{36}$$

Applying (36) to the last three terms of (34) and utilizing the maximum perturbations from Assumption 1 results in

$$\begin{aligned}\dot{V} \leq& -\tilde{\boldsymbol{\eta}}^T\{\mathbf{P}_{1\sigma}\mathbf{K}_{1\sigma} - (1/2\beta)(\Delta\mathbf{A}_{1\sigma} - \mathbf{K}_{2\sigma})^T\mathbf{P}_{2\sigma}\mathbf{H}_\sigma^{-1}\mathbf{P}_{2\sigma}\times\\ &\times(\Delta\mathbf{A}_{1\sigma} - \mathbf{K}_{2\sigma})\}\tilde{\boldsymbol{\eta}} - \tilde{\boldsymbol{\nu}}^T\{\mathbf{P}_{2\sigma}\hat{\mathbf{A}}_{2\sigma} - (3\beta/2)\mathbf{H}_\sigma\}\tilde{\boldsymbol{\nu}}\\ &- \hat{\boldsymbol{\eta}}^T\{\mathbf{P}_{3\sigma}\mathbf{K}_\sigma - (1/2\beta)(\Delta\mathbf{A}_{1\sigma} + \mathbf{K}_{2\sigma})^T\mathbf{P}_{2\sigma}\mathbf{H}_\sigma^{-1}\mathbf{P}_{2\sigma}\times\\ &\times(\Delta\mathbf{A}_{1\sigma} + \mathbf{K}_{2\sigma})\}\hat{\boldsymbol{\eta}}\\ &- \hat{\boldsymbol{\nu}}^T\{\rho_\sigma\mathbf{P}_{4\sigma} - (1/2\beta)\Delta\mathbf{A}_{2\sigma}^T\mathbf{P}_{2\sigma}\mathbf{H}_\sigma^{-1}\mathbf{P}_{2\sigma}\Delta\mathbf{A}_{2\sigma}\}\hat{\boldsymbol{\nu}}\\ &- \rho_{1\sigma}\lambda_{\min}(\mathbf{P}_{4\sigma})||\hat{\boldsymbol{\nu}}||^2 + \tilde{\boldsymbol{\eta}}^T(\mathbf{K}_\sigma + \mathbf{K}_{1\sigma})\hat{\boldsymbol{\eta}} + \tilde{\boldsymbol{\nu}}^T\Delta\mathbf{d}_\sigma.\end{aligned} \tag{37}$$

Observe that $||\boldsymbol{\xi}|| \geq ||\hat{\boldsymbol{\nu}}||$ and $||\boldsymbol{\xi}|| \geq ||\tilde{\boldsymbol{\nu}}||$. Moreover,

$$\alpha\int_0^t ||(\mathbf{K}_{1\sigma} + \mathbf{K}_\sigma)||||\hat{\boldsymbol{\eta}}(\varpi))||||\tilde{\boldsymbol{\eta}}(\varpi)||\mathrm{d}\varpi \geq$$
$$\alpha||(\mathbf{K}_{1\sigma} + \mathbf{K}_\sigma)||||\hat{\boldsymbol{\eta}}(t))||||\tilde{\boldsymbol{\eta}}(t)|| \;\forall t \geq t_0$$

where $\alpha > 1$ by design. Using the design conditions (12)-(14), the fact $\mathbf{P}_{4\sigma} > \mathbf{0}$ and the definitions of $\mathbf{Q}_{i\sigma}$ in (20), we have

$$\begin{aligned}\dot{V} \leq& -\lambda_{\min}(\mathbf{Q}_{1\sigma})||\tilde{\boldsymbol{\eta}}||^2 - \lambda_{\min}(\mathbf{Q}_{2\sigma})||\tilde{\boldsymbol{\nu}}|| - \lambda_{\min}(\mathbf{Q}_{3\sigma})||\hat{\boldsymbol{\eta}}||^2\\ &- \lambda_{\min}(\mathbf{Q}_{4\sigma})||\hat{\boldsymbol{\nu}}||^2 + ||(\mathbf{K}_\sigma + \mathbf{K}_{1\sigma})||||\tilde{\boldsymbol{\eta}}||||\hat{\boldsymbol{\eta}}||\\ &+ ||\tilde{\boldsymbol{\nu}}||||\mathbf{d}_\sigma|| - \rho_{1\sigma}||\hat{\boldsymbol{\nu}}||^2\\ \leq& -\min_i(\lambda_{\min}(\mathbf{Q}_{i\sigma}))||\boldsymbol{\xi}||^2 + ||\Delta\mathbf{d}_\sigma||||\boldsymbol{\xi}||\\ &- ||(\mathbf{K}_\sigma + \mathbf{K}_{1\sigma})||||\tilde{\boldsymbol{\eta}}||||\hat{\boldsymbol{\eta}}||(\alpha||\hat{\boldsymbol{\nu}}||^2 - 1).\end{aligned} \tag{38}$$

The form of V in (22) gives $\varrho_m/2||\boldsymbol{\xi}||^2 \leq V \leq \varrho_M/2||\boldsymbol{\xi}||^2$. Then, for a scalar ζ such that $0 < \zeta < \kappa$, (38) becomes

$$\begin{aligned}\dot{V} \leq& -\zeta V - (\kappa - \zeta)V + ||\Delta\mathbf{d}_\sigma||\sqrt{2V/\varrho_m}\\ &- ||(\mathbf{K}_\sigma + \mathbf{K}_{1\sigma})||||\tilde{\boldsymbol{\eta}}||||\hat{\boldsymbol{\eta}}||(\alpha||\hat{\boldsymbol{\nu}}||^2 - 1).\end{aligned} \tag{39}$$

Further, utilizing the fact $||\boldsymbol{\xi}|| \geq ||\hat{\boldsymbol{\nu}}||$ one has $V \geq (\varrho_m/2)||\boldsymbol{\xi}||^2 \geq (\varrho_m/2)||\hat{\boldsymbol{\nu}}||^2$. Then, noting $\mathcal{B}$ from (23), one can verify that $\dot{V} \leq -\zeta V$ is guaranteed when $V \geq \mathcal{B}$.

In light of this, further analysis is needed to observe the behaviour of $V(t)$ between the two consecutive switching instants, i.e., $t \in [t_l \;\; t_{l+1})$, for two possible scenarios:

- **(i)** when $V(t) \geq \mathcal{B}$, we have $\dot{V}(t) \leq -\zeta V(t)$ implying exponential decrease of the Lyapunov function;
- **(ii)** when $V(t) < \mathcal{B}$, no exponential decrease can be derived.

Behaviour of $V(t)$ is discussed individually for the two cases.

Case (i): There exists a time, call it T_1, when $V(t)$ enters into the bound $\mathcal{B}$ and $N_\sigma(t)$ denotes the number of all switching intervals for $t \in [t_0 \;\; t_0 + T_1)$, where t_0 denotes initial time. Accordingly, for $t \in [t_0 \;\; t_0 + T_1)$, using (33) and $N_\sigma(t_0, t)$ from Definition 1 we have

$$\begin{aligned}V(t) \leq& \mu\exp\left(-\zeta(t - t_{N_\sigma(t)-1})\right)V(t_{N_\sigma(t)-1}^-)\\ \leq& \mu\exp\left(-\zeta(t - t_{N_\sigma(t)-1})\right)\\ &\cdot\mu\exp\left(-\zeta(t_{N_\sigma(t)-1} - t_{N_\sigma(t)-2})\right)V(t_{N_\sigma(t)-2}^-)\\ &\vdots\\ \leq& \mu\exp\left(-\zeta(t - t_{N_\sigma(t)-1})\right)\mu\exp\left(-\zeta(t_{N_\sigma(t)-1} - t_{N_\sigma(t)-2})\right)\\ &\cdots\mu\exp\left(-\zeta(t_1 - t_0)\right)V(t_0)\\ =& \mu^{N_\sigma(t_0,t)}\exp\left(-\zeta(t - t_0)\right)V(t_0)\\ =& b\left(\exp\left(-\zeta + (\ln\mu/\vartheta)\right)(t - t_0)\right)V(t_0),\end{aligned} \tag{40}$$

where $b \triangleq \exp(N_0 \ln\mu)$ is a constant. Substituting the ADT condition $\vartheta > \ln\mu/\zeta$ in (40) yields $V(t) < bV(t_0)$ for $t \in [t_0 \;\; t_0 + T_1)$. Moreover, as $V(t_0 + T_1) < \mathcal{B}$, one has $V(t_{N_\sigma(t)+1}) < \mu\mathcal{B}$ from (33) at the next switching instant $t_{N_\sigma(t)+1}$ after $t_0 + T_1$. This implies that $V(t)$ may be larger than $\mathcal{B}$ from the instant $t_{N_\sigma(t)+1}$: however, using a recursive argument as in [28], we can come to the conclusion that $V(t) < b\mu\mathcal{B}$ for $t \in [t_0 + T_1 \;\; \infty)$.

Case (ii): It can be easily verified that the same argument below (40) also holds for Scenario (ii).

Thus, observing the stability arguments of the Case (i) and (ii), the GUUB result (23) can be concluded, which further implies $\tilde{\boldsymbol{\eta}}, \tilde{\boldsymbol{\nu}}, \hat{\boldsymbol{\eta}}, \hat{\boldsymbol{\nu}} \in \mathcal{L}_\infty \Rightarrow \boldsymbol{\eta}, \boldsymbol{\nu} \in \mathcal{L}_\infty$.

REFERENCES

[1] O. Levander, "Autonomous ships on the high seas," *IEEE Spectrum*, vol. 54, no. 2, pp. 26–31, 2017.

[2] A. Veksler, T. A. Johansen, F. Borrelli, and B. Realfsen, "Dynamic positioning with model predictive control," *IEEE Transactions on Control Systems Technology*, vol. 24, no. 4, pp. 1340–1353, July 2016.

[3] C. Paliotta, E. Lefeber, K. Y. Pettersen, J. Pinto, M. Costa *et al.*, "Trajectory tracking and path following for underactuated marine vehicles," *IEEE Transactions on Control Systems Technology*, no. 99, pp. 1–15, 2018.

[4] J. Flint and R. Stephens, "Dynamic positioning for heavy lift applications," in *Dynamic Positioning Conference, Houston*. Marine Technology Society, 2008, pp. 1–10.

[5] H. Chen, T. Moan, and H. Verhoeven, "Safety of dynamic positioning operations on mobile offshore drilling units," *Reliability Engineering & System Safety*, vol. 93, no. 7, pp. 1072 – 1090, 2008.

[6] F. Bakker, "A conceptual solution to instable dynamic positioning during offshore heavy lift operations using computer simulation techniques," Master's thesis, TU Delft, The Netherlands, 2015.

[7] B. Rokseth, I. B. Utne, and J. E. Vinnem, "A systems approach to risk analysis of maritime operations," *Proceedings of the Institution of Mechanical Engineers, Part O: Journal of Risk and Reliability*, vol. 231, no. 1, pp. 53–68, 2017.

[8] S. Minsaas, Stuart, V. Joshi, and G. Haldipur. (2014) Careful planning precedes successful platform installation at ekofisk. [Online]. Available: https://www.offshore-mag.com/home/article/16804666/careful-planning-precedes-successful-platform-installation-at-ekofisk

[9] Heerema Marine Contractors. (2019) Thialf. [Online]. Available: https://hmc.heerema.com/fleet/thialf/

[10] D. A. Smallwood and L. L. Whitcomb, "Model-based dynamic positioning of underwater robotic vehicles: theory and experiment," *IEEE Journal of Oceanic Engineering*, vol. 29, no. 1, pp. 169–186, 2004.

[11] S. Heshmati-alamdari, G. C. Karras, P. Marantos, and K. J. Kyriakopoulos, "A robust model predictive control approach for autonomous underwater vehicles operating in a constrained workspace," in *2018 IEEE International Conference on Robotics and Automation (ICRA)*. IEEE, 2018, pp. 1–5.

[12] S. Küchler, T. Mahl, J. Neupert, K. Schneider, and O. Sawodny, "Active control for an offshore crane using prediction of the vessel's motion," *IEEE/ASME Transactions on Mechatronics*, vol. 16, no. 2, pp. 297–309, 2011.

[13] X. Hu and J. Du, "Robust nonlinear control design for dynamic positioning of marine vessels with thruster system dynamics," *Nonlinear Dynamics*, pp. 1–12, 2018.

[14] Y. Wang, Y. Tuo, S. X. Yang, M. Biglarbegian, and M. Fu, "Reliability-based robust dynamic positioning for a turret-moored floating production storage and offloading vessel with unknown time-varying disturbances and input saturation," *ISA Transactions*, 2018.

[15] Z. Sun, G. Zhang, L. Qiao, and W. Zhang, "Robust adaptive trajectory tracking control of underactuated surface vessel in fields of marine practice," *Journal of Marine Science and Technology*, pp. 1–8, 2018.

[16] W.-Z. Yu, H.-X. Xu, and H. Feng, "Robust adaptive fault-tolerant control of dynamic positioning vessel with position reference system faults using backstepping design," *International Journal of Robust and Nonlinear Control*, vol. 28, no. 2, pp. 403–415, 2018.

[17] X. He, W. He, J. Shi, and C. Sun, "Boundary vibration control of variable length crane systems in two-dimensional space with output constraints," *IEEE/ASME Transactions on Mechatronics*, vol. 22, no. 5, pp. 1952–1962, 2017.

[18] X. Lin, J. Nie, Y. Jiao, K. Liang, and H. Li, "Nonlinear adaptive fuzzy output-feedback controller design for dynamic positioning system of ships," *Ocean Engineering*, vol. 158, pp. 186–195, 2018.

[19] A. Witkowska and R. Śmierzchalski, "Adaptive dynamic control allocation for dynamic positioning of marine vessel based on backstepping method and sequential quadratic programming," *Ocean Engineering*, vol. 163, pp. 570–582, 2018.

[20] N. Sun, Y. Fang, H. Chen, and B. He, "Adaptive nonlinear crane control with load hoisting/lowering and unknown parameters: Design and experiments," *IEEE/ASME Transactions on Mechatronics*, vol. 20, no. 5, pp. 2107–2119, 2015.

[21] S. Messineo and A. Serrani, "Offshore crane control based on adaptive external models," *Automatica*, vol. 45, no. 11, pp. 2546–2556, 2009.

[22] J. Du, X. Hu, M. Krstić, and Y. Sun, "Dynamic positioning of ships with unknown parameters and disturbances," *Control Engineering Practice*, vol. 76, pp. 22–30, 2018.

[23] J.-M. Godhavn, T. I. Fossen, and S. P. Berge, "Non-linear and adaptive backstepping designs for tracking control of ships," *International Journal of Adaptive Control and Signal Processing*, vol. 12, no. 8, pp. 649–670, 1998.

[24] S. A. Værnø, R. Skjetne, Ø. K. Kjerstad, and V. Calabrò, "Comparison of control design models and observers for dynamic positioning of surface vessels," *Control Engineering Practice*, vol. 85, pp. 235–245, 2019.

[25] T. I. Fossen, *Handbook of marine craft hydrodynamics and motion control*. John Wiley & Sons, 2011.

[26] J. Ye, M. Godjevac, S. Baldi, and H. Hopman, "Joint estimation of vessel position and mooring stiffness during offshore crane operations," *Automation in Construction*, vol. 101, pp. 218–226, 2019.

[27] J. P. Hespanha and A. S. Morse, "Stability of switched systems with average dwell-time," in *Proceedings of the 38th IEEE Conference on Decision and Control*.

[28] S. Roy and S. Baldi, "A simultaneous adaptation law for a class of nonlinearly-parametrized switched systems," *IEEE Control Systems Letters*, vol. 3, no. 3, pp. 487–492, 2019.

[29] ——, "On reduced-complexity robust adaptive control of switched euler–lagrange systems," *Nonlinear Analysis: Hybrid Systems*, vol. 34, pp. 226–237, 2019.

[30] S. Yuan, B. De Schutter, and S. Baldi, "Robust adaptive tracking control of uncertain slowly switched linear systems," *Nonlinear Analysis: Hybrid Systems*, vol. 27, pp. 1–12, 2018.

[31] T. I. Fossen and A. Grovlen, "Nonlinear output feedback control of dynamically positioned ships using vectorial observer backstepping," *IEEE Transactions on Control Systems Technology*, vol. 6, no. 1, pp. 121–128, 1998.

[32] G. Lai, Z. Liu, Y. Zhang, C. P. Chen, and S. Xie, "Adaptive backstepping-based tracking control of a class of uncertain switched nonlinear systems," *Automatica*, vol. 91, pp. 301–310, 2018.

[33] T. Fossen and T. Perez, "Marine systems simulator (mss)," https://github.com/cybergalactic/MSS, accessed 2004.

[34] H. K. Khalil and J. Grizzle, *Nonlinear systems*. Prentice hall Upper Saddle River, NJ, 2002, vol. 3.